

Article

Using Remote Sensing to Assess the Vegetation Cover of a Protected Salt Marsh Subjected to Artificial Recharge and Groundwater Abstractions during the Period 1925–2022 (Alicante, SE Spain)

José Marín Salcedo ¹, Iván Alhama ¹, Manuel Alcaraz ¹, José Álvarez-Rogel ² and José Antonio Jiménez-Valera ^{1,*}

¹ Mining and Civil Engineering Department, Technical University of Cartagena, Paseo de Alfonso XIII 52, 30203 Cartagena, Spain; jose.marin@upct.es (J.M.S.); ivan.alhama@upct.es (I.A.); m.alcaraz@upct.es (M.A.)

² Department of Agricultural Engineering of the E.T.S.I.A., Soil Ecology and Biotechnology Unit of the Institute of Plant Biotechnology, Technical University of Cartagena, 30203 Cartagena, Spain; jose.alvarez@upct.es

* Correspondence: jose.jvalera@upct.es

Abstract: The Agua Amarga salt marsh has been subjected to artificial seawater recharge on its surface during the period 1925–1969 for industrial purposes (saltwork activity) and from 2008 to present to compensate for coastal groundwater abstraction to supply Alicante desalination plants. This groundwater abstraction has caused piezometric depletion in the coastal aquifer connected to the protected salt marsh. The seawater recharge program also involved vegetation monitoring to control the impact on the salt marsh ecosystem, allowing data to be collected about the halophyte vegetation species growing in the salt marsh (*Arthrocnemum macrostachyum*, *Sarcocornia fruticosa*, and *Ruppia maritima*, among others) from spring and autumn field surveys. In this work, vegetation development is assessed with remote sensing for the period 1929–2022 using images with visible and near-infrared spectral resolution. Different spectral indices (NDVI, BI, and NDWI) and classification algorithms (random forest) are used to calculate the vegetation cover. Field data are employed to evaluate the protocols and compare the results, showing a 46% decrease caused by the salt works and a 50% increase as a result of natural evolution and artificial recharge. The spread of *Phragmites australis* is also addressed by comparing LiDAR data with field monitoring, showing an increase of 12% during the period 2005–2023. The advantages and complementarity of field monitoring and remote sensing information are explained.

Keywords: coastal aquifer; artificial recharge; vegetation cover; remote sensing; GIS; reedbed



Citation: Salcedo, J.M.; Alhama, I.; Alcaraz, M.; Álvarez-Rogel, J.; Jiménez-Valera, J.A. Using Remote Sensing to Assess the Vegetation Cover of a Protected Salt Marsh Subjected to Artificial Recharge and Groundwater Abstractions during the Period 1925–2022 (Alicante, SE Spain). *Sustainability* **2024**, *16*, 973. <https://doi.org/10.3390/su16030973>

Academic Editors: Yen-Ming Chiang, Wen-Ping Tsai and Yu-Jia Chiu

Received: 31 December 2023

Revised: 19 January 2024

Accepted: 21 January 2024

Published: 23 January 2024



Copyright: © 2024 by the authors. Licensee MDPI, Basel, Switzerland. This article is an open access article distributed under the terms and conditions of the Creative Commons Attribution (CC BY) license (<https://creativecommons.org/licenses/by/4.0/>).

1. Introduction

Over the last hundred years, the evolution of the Agua Amarga salt marsh (south of the city of Alicante, Spain) has been influenced by anthropogenic interventions. Some of them have modified the environmental conditions, while others have been carried out to control the impact of human activities.

During the last 15 years, the combination of groundwater resource exploitation to supply desalination plants and the sea water irrigation plan over the protected salt marsh has been considered an environmentally sustainable human intervention in the Agua Amarga salt marsh and the connected coastal aquifer. Thus, the irrigation program has had positive effects on the salt marsh.

But protecting living ecosystems means facing challenges due to climate fluctuations. The Isolated Depressions at High Levels that have occurred during the last decade in the southeastern Iberian Peninsula [1,2], such as events in December 2016–January 2017, April 2019, August–September 2019, and March 2022, have caused exceptional precipitation

(Figure 1). Discharging surface water from the storm storage tank at the Alicante Airport located to the south of the salt marsh (Figure 2) led to a sporadic sheet of fresh water on the ponds in the southern part of the salt marsh. This caused extensive proliferation of *Phragmites australis* (common reed) in the south, far from the seawater irrigation ponds, as well as the growth of invasive plant species such as *Nicotiana glauca*, *Conyza bonariensis*, *Aster squamatus*, and *Centaurea seridis*, among others.

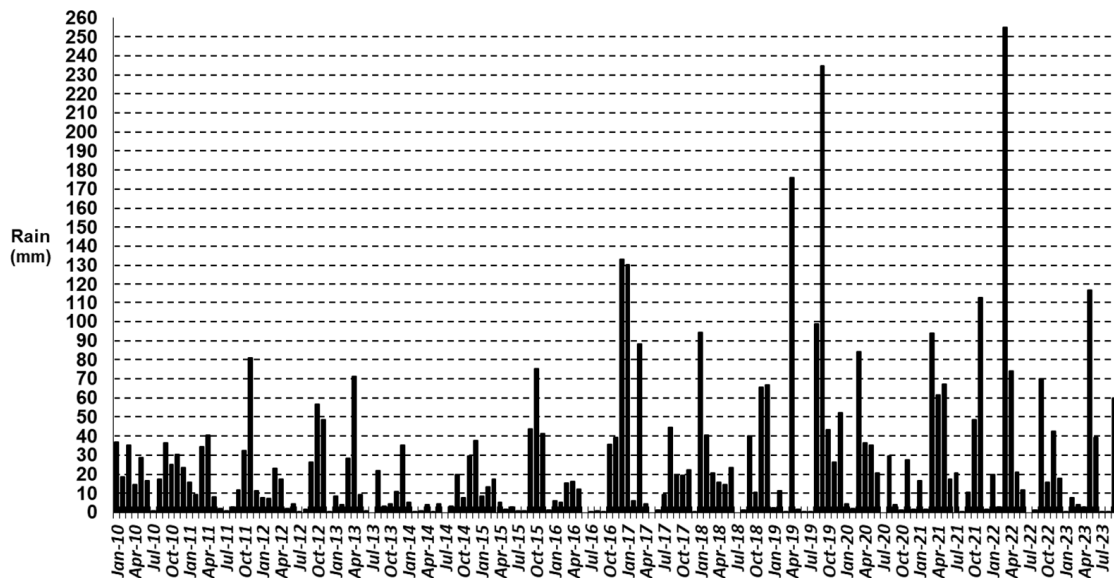


Figure 1. Monthly rain distribution in the study area. Data collected from the Alicante Airport weather station [3].

One of the effects of fresh water on the ecosystem and the subsequent diminishing of salt in soils and aquifers is the spreading of the reedbed. The common reed is an invasive species under special environmental surveillance [4]. To understand the global impact of this problem and its interconnection to the ecosystem, some examples can be highlighted. Gagnon Lupien et al. [5] established that the Eurasian genotype of the common reed is quickly invading freshwater marshes in North America. Since some bird species depend on certain plant stands for feeding and breeding, they could be negatively affected by the spread of this invader. According to Tougas-Tellier et al. [6], low water levels in several river systems make wetlands particularly vulnerable to the spread of invasive species, such as the common reed (*Phragmites australis*). The authors developed a model to map the distribution of potential common reed germination grounds in the freshwater wetlands of the St. Lawrence River (Quebec, Canada) under current climatic conditions. They then used this model to predict their future distribution under two simulated climate change scenarios for 2050. They also collected historical and recent remotely sensed data on common reed distribution to calibrate and validate the model. Although some authors consider reedbeds to be a key attribute of many wetlands [7], they generally pose a risk to native salt marsh species.

Accurate, up-to-date information on the distribution and status of the reedbed is difficult to obtain through field surveys because reedbeds exist as small, sparsely distributed patches across the landscape [8]. Moreover, in large areas, field surveys are difficult, time-consuming, and expensive to conduct [9]. The spread of *Phragmites australis* also densifies the vegetation, impeding access to specific soil and vegetation control points during the field surveys. In addition, the presence of arachnid-like ticks (*Parasitiformes ixodoidea*) makes collecting data risky for field survey technicians, especially in spring. These situations have prompted us to search for alternatives to monitor the ecosystem. In this work, we present a system of remote sensing and image processing using an open-source database that is free for researchers [10].

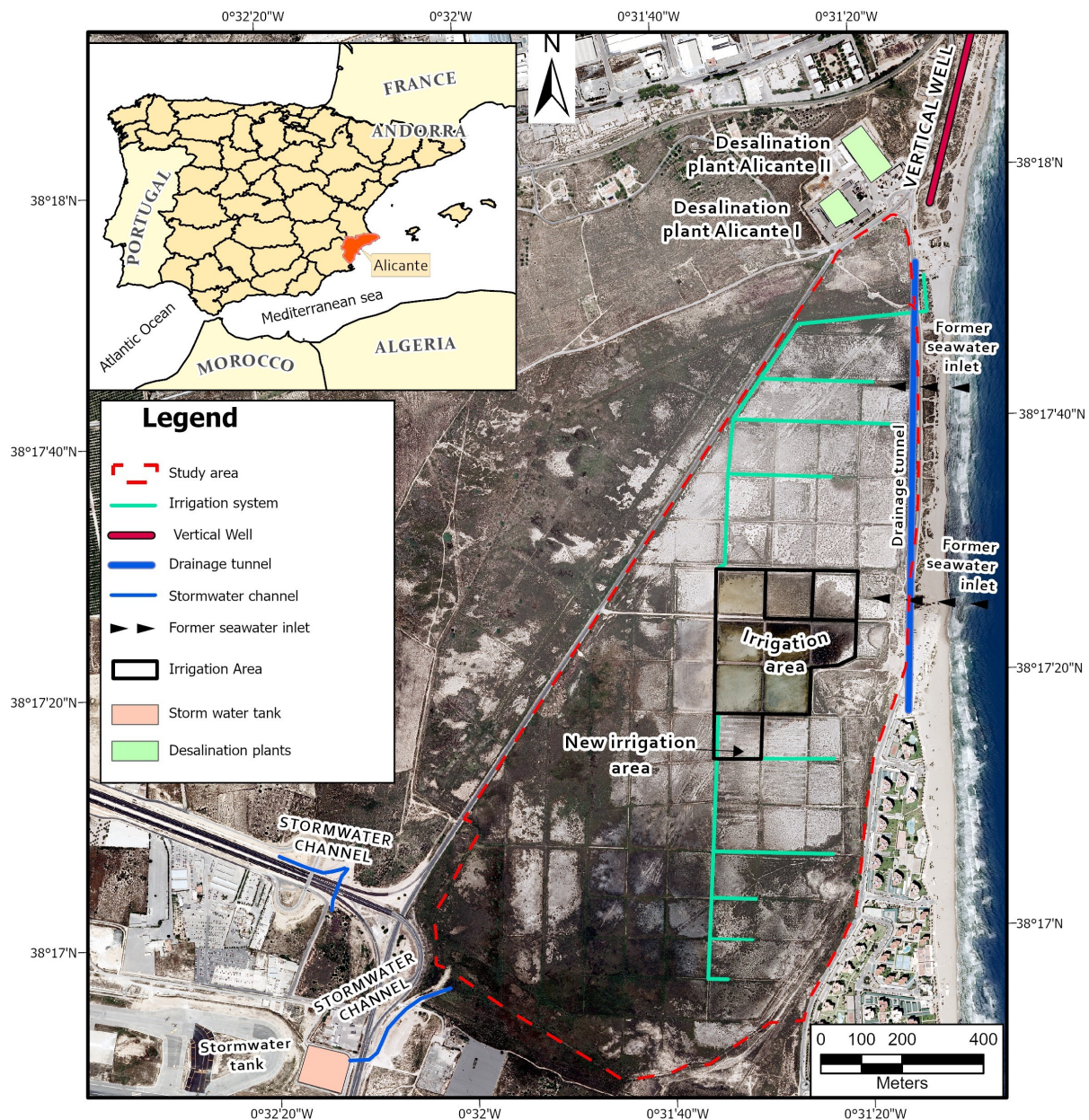


Figure 2. Location of the Agua Amarga salt marsh.

Remote sensing and image processing mapping have been widely applied in the environmental sciences since the beginning of their development [11], and they continue to be employed in works on water management and vegetation cover. For example, to reduce water scarcity in arid regions, remote sensing and GIS techniques have been successfully applied to predict areas with potential water resources [12,13]. Combined remote sensing, GIS (Geographic Information System)-based frequency ratios, and evidential belief delineate and quantify prospective groundwater areas in a model.

Regarding vegetation studies, many applications have been carried out all over the world. In Yaqui Valley, Mexico, remote sensing was applied to understand yield variations in irrigation wheat fields [14]. Processed satellite images using GRASS (Geographic Resources Analysis Support System) and GIS have been employed in the mangroves of the Niger Delta (Nigeria) to survey the rapid decline of mangrove habitats since the estuary is a biodiversity hotspot submitted to climatic problems and anthropogenic factors [15]. Jamali et al. [16] predicted the expansion of salinity in the Golpayegan Plain by estimating

vegetation cover and wetland area losses using Landsat images from 1985 to 2016. The Soil Salinity Index (SSI) and Normalized Difference Vegetation Index (NDVI) were deduced from the Landsat images. Tiwari et al. [17] identified the transplanting date, peak vegetative growth stage, and harvest dates of rice in the Nagarjuna Sagar and Krishna Delta System areas. Their objective was to help schedule and optimize the use of irrigation water released from the reservoir to the command areas.

The aim of this work is to validate remote sensing images with visible and near-infrared spectral resolution and high spatial resolution as an alternative way to assess the evolution of vegetation cover and as a complement to vegetation field monitoring. The importance of combining both methodologies has been largely reported in previous studies [9,18], among them some concerning salt marshes. Applying this technique to the Agua Amarga salt marsh has made it possible to study the periods lacking information (1929–1977) using unsupervised classification algorithms and to gather data not observed in field surveys. This technique was used in the quantified mapping of the salt marsh vegetation in the lagoon of Venice (Italy) [19]. The validation of field data during the artificial recharge program (2008–2022) was conducted with supervised algorithms. The selection criteria for the different indices depend on the original image and purpose [20,21]. We chose the Normalized Difference Vegetation Index (NDVI) [22] and the Normalized Difference Water Index (NDWI) [23] for this period. Handheld field spectrometers were not used in this study, which would have contributed to better calibrated images [20].

Classifying species with the derived digital elevation model is also an aspect we dealt with in this work. LiDAR data, which has been previously applied to monitor species classification in salt marshes [24], was used to address the spread of *Phragmites australis* [9,25].

Two pilot ponds have been analyzed, one located next to the artificially irrigated area and the other in the south, near the area affected by freshwater. We aim to assess the influence of water on permanent and seasonal vegetation growth. Several procedures have been developed, such as algebraic operations between the different spectral bands and supervised classification algorithms [19]. Field data have been used to evaluate the protocols, and the results from different methodologies have been represented in graphs.

2. Materials and Methods

In this section, after describing the study area, we deal with two different types of procedures: those related to field surveys and those linked to aerial image processing.

2.1. Study Area

The Agua Amarga salt marsh is an endoreic lagoon formed during the Neogene-Quaternary period. It is separated from the sea by sand dunes from the Holocene. Nowadays, in the surrounding 180 ha occupied by the salt marsh, there are some human infrastructures, like the groundwater abstraction system of desalination plants or the stormwater tank at the Alicante airport (Figure 2), which require water management measures and environmental surveillance.

Between 1925 and 1969, the surface of the current salt marsh was used for solar salt works [26]. As shown in Figure 3, the landscape was gradually transformed to settle the evaporation ponds. Figure 3a shows the beginning of this activity, with part of the study area occupied and active and the other with natural vegetation. Figure 3b shows fully operational salt work activity, and Figure 3c was taken eight years after the salt works were abandoned, with signs of vegetation recovery beginning to emerge. The outlines of the ponds, each of which is around 1200 m², can be seen in the aerial images. As a result of this activity, the vegetation cover diminished, and the aquifer was affected by salt contamination.

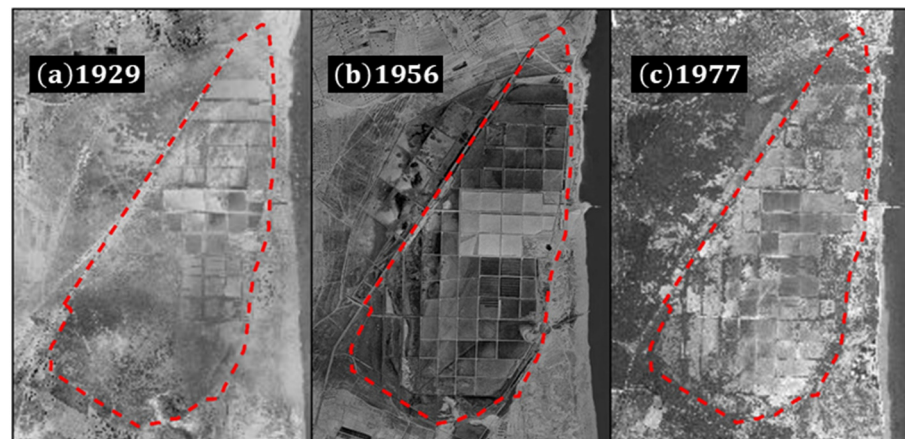


Figure 3. Evolution of the landscape altered by the salt work industry during the period 1929–1977. The red contour line indicates the study area. Images from (a) 1929, Ruiz de Alda Flight [27], (b) 1956, American Flight [28], and (c) 1977, Interministerial Flight [29].

After that period, the salt marsh evolved naturally as an endoreic lagoon subject to periods of flooding due to the accumulation of surface water or the rise of the piezometric level. An area of 207.75 ha, of which 140.28 ha is included in the study area (Figure 2), was declared a protected wetland in 2002 and included in the Valencia Community wetland catalog [30]. Its coastline, part of the Tabarca Island Marine Reserve, is a Site of Community Interest (SCI) and a Special Protection Area (SPA) for Birds, hosting EU-protected habitats. Figure 4a shows the aerial orthophotography in 2005 after this period of natural evolution. The outline of the ponds had been partially obscured due to vegetation growth, though the presence of salt could still be perceived in most of them.

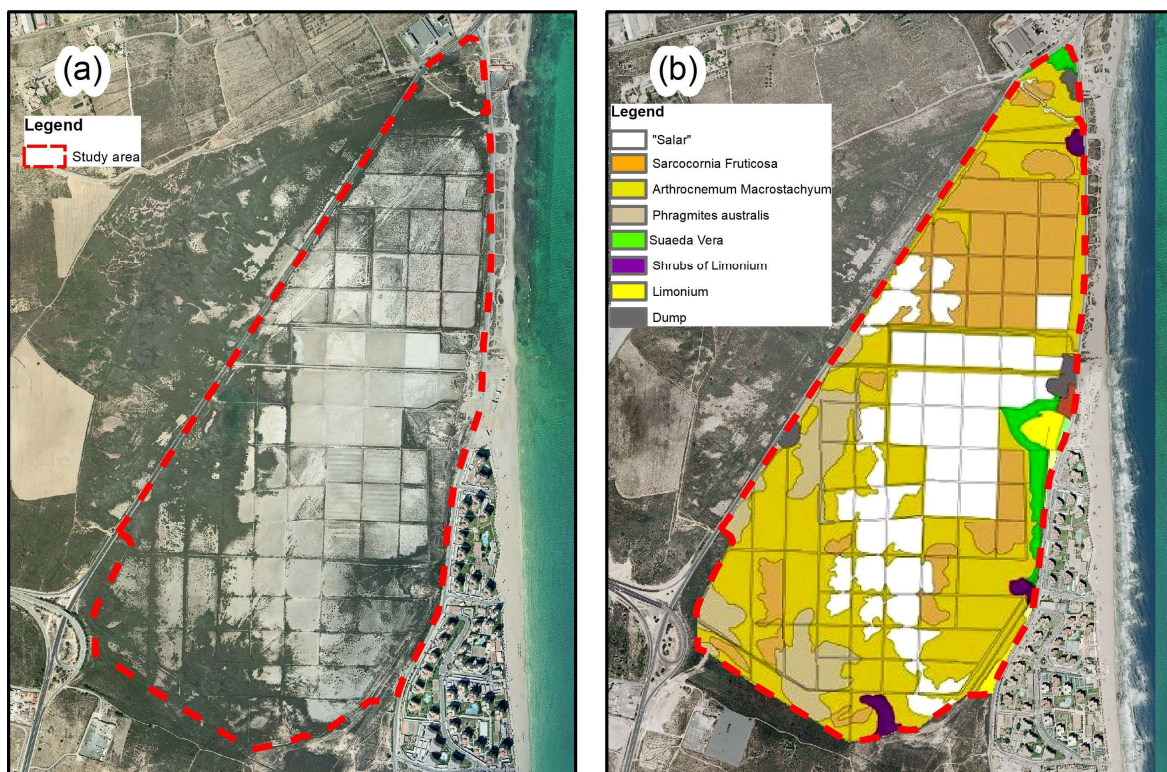


Figure 4. (a) Aerial orthophotography from 2005 showing the vegetation spread over the salt marsh after 36 years of natural evolution and 3 years before the beginning of the seawater recharge program [31]. (b) Vegetation map according to Rodríguez Estrella et al. [32].

To determine the basis of the vegetation species distribution for subsequent monitoring before performing the next human intervention, the environmental study impact report for the desalination plants project carried out in 2005 included the vegetation map shown in Figure 4b [32]. For the first time, a field survey was performed to define the vegetation cover and main species in the salt marsh. *Arthrocnemum macrostachyum* and *Sarcocornia fruticosa* were among the predominant species (in gold and orange in Figure 4b). The area without vegetation was also depicted. This area is called “salar” (a salt flat or salt-encrusted plain) since salt crystals could be found on the surface (in white in Figure 4b).

Since 2005, the coastal aquifer located below the salt marsh and along the coastline has been used to supply the Alicante I Desalination Plant, pumping groundwater from vertical wells. Since 2008, the Alicante II Desalination Plant has been abstracting groundwater along the coast through a one-kilometer-long drainage tunnel system located between the salt marsh and the sea and eight horizontal directional drilling wells [33]. As a result, the Agua Amarga coastal aquifer has experienced piezometric depletion below its surface. To mitigate the impact on the salt marsh ecosystem and manage the coastal aquifer, a superficial seawater irrigation program was set up to reduce the groundwater level drawdown and contribute to conserving the halophyte-protected species. To this end, a seawater pipe system was outlined to cover 35 pods, equivalent to 33.1% of the study area (Figure 2). An economic study of this measure was carried out by Navarro and Sanchez Lizaso [34].

Using seawater as a viable alternative was justified due to the salinity in the groundwater caused by the previous salt work activity (reaching up to 300 mS/cm according to Manteca et al. [35]) and the existence of halophyte species and salt in the soils (reaching up to 14 mS/cm according to Gonzalez-Alcaraz [36]).

The irrigation project continues to this day. It was funded by the owner of the desalination plants, the Mancomunidad de los Canales del Taibilla, a water management body of the Spanish Government. Since 2008, the Technical University of Cartagena has been monitoring the aquifer, the soils, and the vegetation cover to document the sustainability of this project involving groundwater resource exploitation and ecosystem preservation. Field surveys have been carried out every month to evaluate the management of the aquifer and every six months to monitor soil and vegetation. The existence of Halophilous shrubs of *Suaeda vera* and *Limonium* sp., steppe grass *Lygeum spartum*, and stands of halophytes *Sarcocornia fruticosa* and *Arthrocnemum macrostachyum*, recognized as typical salt marsh vegetation, increased 10–25% in the area occupied during the period 2012–2020 [37]. Regarding groundwater management, the aquifer connection with the sea through the Holocene and Pliocene sands and conglomerates and the proximity of the pumping system to the coastline guaranteed the supply of seawater. The seawater recharge program stabilized the falling piezometry in the salt marsh, with the depression cone and saltwater intrusion limited to the coastline, as can be seen in the piezometric contour lines depicted in the map in Figure 5. The recharge program also contributed to reducing the salinity in the aquifer, around 150 mS/cm below the salt marsh during the period 2012–2022, to values very close to seawater [37].

2.2. Field Surveys

In the spring of 2012, 63 sampling plots were located throughout the salt marsh to evaluate the percentage of vegetation cover (visual estimation) [36]. Once a year, 21 plots are selected to be visited during the field survey. There, the observation regarding vegetation evolution is manually recorded on a paper map. Later, the map is digitalized, and the vegetation cover map is made using interpolation with GIS (see Figure 3b). This methodology considers the predominance of species but does not contemplate the soil without vegetation between nearby specimens.

To specifically identify the extent of *Phragmites australis* in October 2023, a field survey with GPS Equipment was carried out (Figure 6). We used a GPS with an AS10 antenna, working in RTK (real-time kinematic) with the ERVA network (Geodetic network of reference stations in Valencia). The horizontal accuracy was 1 cm (+1 ppm), and the vertical

accuracy was 2 cm (+1 ppm). The area where *Phragmites australis* was the predominant species (denominated intensive reedbed) was separated from the area where it was absent, insignificant, or the plants were young specimens (Figure 6). Young plants could be potential areas for future spreading.

The data collected during the field monitoring from 2005 to 2023 were used to compare the evolution of the areas with vegetation and the spread of the reedbed, with the result obtained via image processing.

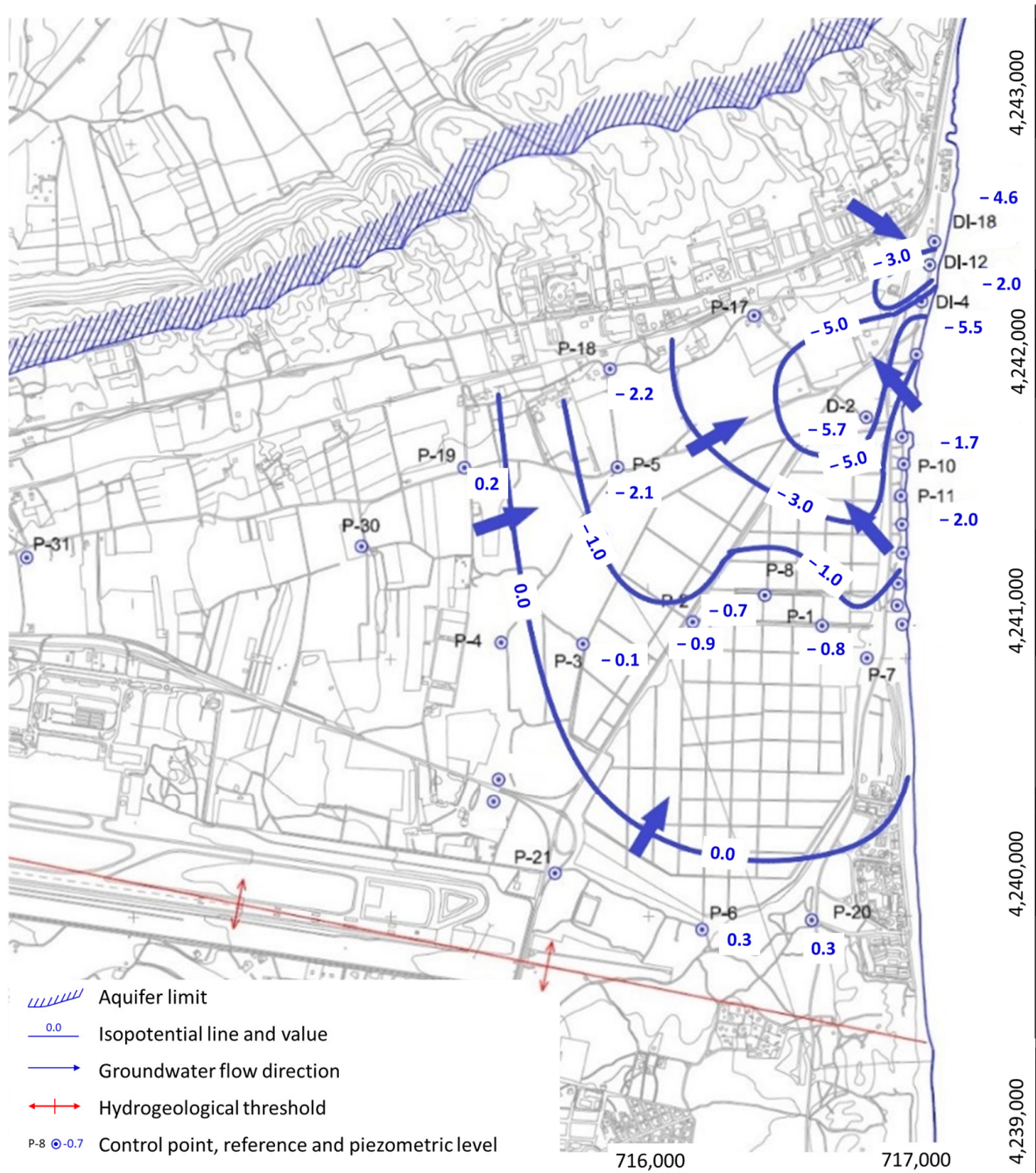


Figure 5. Piezometric map from 19 July 2023. Seawater intrudes on the aquifer along the coastline to the abstraction system of the Alicante I and II desalination plants (depletion around -5.5 m a.s.l.), while the aquifer recharge over the salt marsh avoids piezometric depletion below the salt marsh (piezometry around -1.0 m a.s.l.).

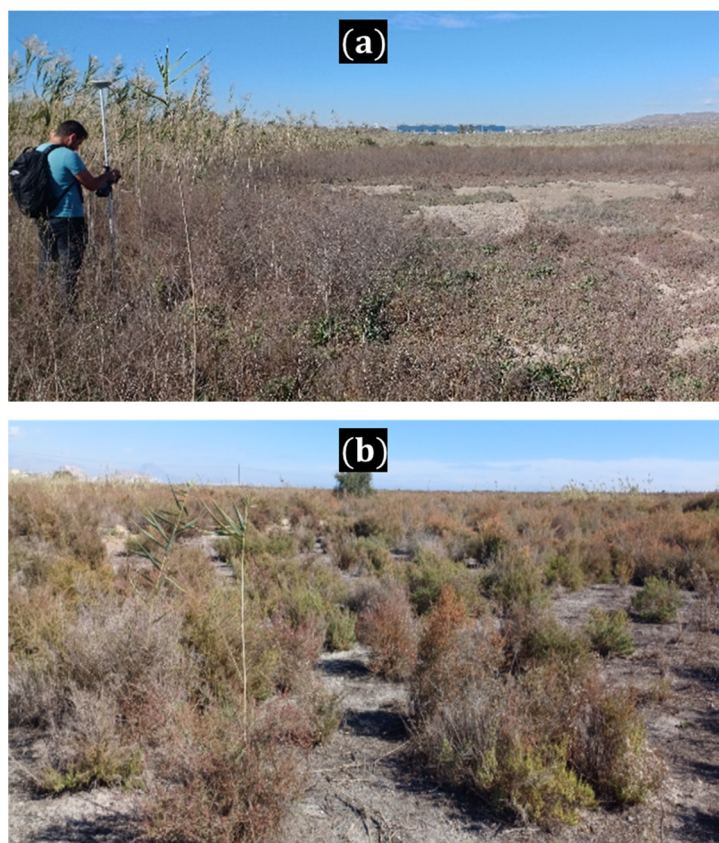


Figure 6. Marking *Phragmites australis* during the field survey in October 2023. (a) Sharp boundary between a dense stand of *Phragmites australis* and the halophytic vegetation dominated by the succulent shrub *Sarcocornia fruticosa*. (b) Shoots of *Phragmites australis* growing among *Sarcocornia fruticosa* plants and two young specimens of *Phragmites australis*.

2.3. Image Processing

To analyze the first period of historical orthophotos (1929–1956, Figure 3), the images were digitalized using GIS, and the area occupied by evaporation ponds was assumed to be without vegetation cover. The extension was calculated using photointerpretation enhanced with image segmentation [38]. The rest of the study area was considered natural vegetation cover (the area outside the evaporation ponds).

For the second period of historical orthophotos (1977–2005, Figures 3 and 4b), the methodology is automated with an unsupervised classification using the ISO cluster algorithm with ArcGis Pro 3.1 [39], with a minimum class size of 20 and a sampling interval of 10. Minor editing with GIS was applied to calculate vegetation cover [40]. The vegetation cover map of 2005 (Figure 4b) has been digitized and georeferenced using GIS processing.

The methodology applied to the images that include the information from 4-band RGBI, corresponding to red, green, blue, and near infrared (NIR) airborne imagery, is divided into three phases: (i) image pre-processing, in which acquisition, radiometric normalization, and cropping have been carried out for the study area; (ii) the calculation of the vegetation, soil, and water index, and composition of an image with all the bands; and (iii) the classification and control of the results obtained from a confusion matrix. The spatial resolution is 50 cm for the year 2007 and 25 cm for the rest (2017, 2019, and 2022). Although the images are the same type (Aerial image/RGBI from PNOA and IDEV sources, Table 1), they were obtained from different remote cameras located in the aerial devices. The resolution of these cameras was improved from 2007 to 2017. In the case of the Valencian Community, the information is provided annually.

Table 1. Information from aerial images used to study the vegetation cover during the period 1929–2022 in the Agua Amarga salt marsh (Alicante, SE Spain).

| Time | Source of the Image | Type of Information | Working Methodology | Purpose |
|-----------------------------|-------------------------------------------------------------|-----------------------------------------------------------------------------|-----------------------------------------------------------------------------------------------|---------------------------------------------------------------------------------------------------|
| 1929 | Historical Ruiz de Alda Flight (CHS *) | Aerial image/Panchromatic/1 m spatial resolution | Segmentation and enhancement with photointerpretation with delineation of the ponds in GIS | % of area occupied by salt ponds (soil without vegetation) |
| 1956 | Historical American Flight (IGN *) | Aerial image/Panchromatic/1 m spatial resolution | Segmentation and enhancement with photointerpretation with delineation of the ponds in GIS | % of area occupied by salt ponds (soil without vegetation) |
| 1977 | Historical Interministerial Flight (CHS) | Aerial image/Panchromatic/1 m spatial resolution | Unsupervised classification with minor editing (GIS) | % of area occupied by vegetation |
| 2005 From 3/09 to 05/11 | (PNOA * and IDEV *) | Aerial image/RGB */ 0.5 m spatial resolution | Unsupervised classification with minor editing (GIS) | % of area occupied by vegetation |
| 2005 | Vegetation distribution map, Rodríguez Estrella et al. [32] | Map | GIS processing to calculate the surface area of each species and the soils without vegetation | % of area occupied by <i>Phragmites australis</i> , % of area occupied by soil without vegetation |
| 2007 From 23/08 to 03/09 | (PNOA and IDEV) | Aerial image/RGBI * (in nm 630, 560, 470, and 740)/0.5 m spatial resolution | Supervised classification (random forest) | % of area occupied by vegetation |
| 2017 From 08/06 to 23/08 | (PNOA and IDEV) | Aerial image/RGBI (in nm, 620, 530, 430, and 720)/0.25 m spatial resolution | Supervised classification (random forest) | % of area occupied by vegetation |
| 2019 From 14/05 to 30/06 | (PNOA and IDEV) | Aerial image/RGBI (in nm, 620, 530, 430, and 720)/0.25 m spatial resolution | Supervised classification (random forest) | % of area occupied by vegetation |
| 2022 From 08/05 to 11/06 | (PNOA and IDEV) | Aerial image/RGBI (in nm, 610, 520, 470 and 720)/0.25 m spatial resolution) | Supervised classification (random forest) | % of area occupied by vegetation. |
| 2009 | PNOA with LiDAR sensor (1st coverage 2008–2015)/IGN * | nDSM of vegetation-/2.5 m spatial resolution | GIS processing for calculation of maximum vegetation height and occupied surface area | % Identification of tall plant species |
| 2016 | PNOA with LiDAR sensor (2nd coverage 2015-present)/IDEV | nDSM of vegetation/1 m spatial resolution | GIS processing for calculation of maximum vegetation height and occupied surface area | % Identification of tall plant species |

* Segura Hydrographic Confederation; IGN: Spanish National Geographic Institute; PNOA: Spanish National Plan for Aerial Orthophotography; IDEV: Valencian Spatial Data Infrastructure; RGB: Red Green Blue; RGBI: Red Green Blue near Infrared; nDSM: Normalized Digital Surface Model.

Once the images of the four sheets of the different years were downloaded, a mosaic was made. Since the 4 images from the same year have the same spatial resolution (0.5 m for 2007 and 0.25 m for 2017, 2019, and 2022), the mosaic procedure was carried out easily and directly, and the images were ready to be used. After being geometrically corrected, the final image was obtained, and a new raster was generated, where the study area was determined by cutting with ArcGis Pro 3.1. One aspect of PNOA orthophotographs is that their purpose is visualization, so they have been made with different sensors over the course of a year. The quality of these sensors has improved over time, although they were not initially prepared for remote sensing processing. Subsequently, an ArrNorm plugin of QGIS processing was applied to perform radiometric normalization using the Iteratively Reweighted Multivariate Alteration Detection (IRMAD) method. This procedure, proposed by Canty and Nielsen in 2008 [41], facilitates automatic radiometric normalization of multispectral and hyperspectral images. It is achieved by identifying optimal linear

combinations between target image bands and a reference image, leading to the creation of normalized image pairs via canonical correlation analysis. This method assumes that reflectivity values in consistent areas of a scene are invariant between different temporal captures. The reference image used for normalization corresponded to the year 2020, which was not included in the subsequent classification phases.

Once we normalized the PNOA images, we calculated different indexes that, combined with the spectral information of the image bands themselves, increased the accuracy when classifying the images [21]. For this purpose, the following indices have been calculated using the SNAP software (Sentinel Applications Platform, Sentinel 1): the NDVI [22], which is a measure of photosynthetic activity and is strongly correlated with vegetation density and vitality; the NDWI [23], which is complementary to the previous one and indicates the water status of the vegetation; and finally, the Brightness Index (BI) [42], which is sensitive to soil luminosity and is highly correlated with humidity and the presence of salts on the surface. The indices were calculated using the following formulas:

$$\text{NDVI} = \frac{\text{Nir} + \text{Red}}{\text{Nir} - \text{Red}} \quad (1)$$

$$\text{BI} = \sqrt{\frac{\text{Red}^2 + \text{Green}^2}{2}} \quad (2)$$

$$\text{NDWI} = \frac{\text{Green} - \text{Nir}}{\text{Green} + \text{Nir}} \quad (3)$$

These indices were subsequently combined into a single image composed of seven bands (R, G, B, I, NDVI, BI, and NDWI). It provides a representation integrating aspects of vegetation, soil, and moisture.

The categories have been defined at two levels of disaggregation: the vegetation and soil macroclass levels. Each one is divided into two class levels: dense vegetation and sparse vegetation and bare soil and bare dark soil. Using the same spectral indices in all of the images, an unsupervised classification was made with ISO clustering and field data and photointerpretation reinforcement. Forty training and control regions were chosen, with 75% used for training and 25% for validation.

Using the defined training regions and the images composed of the seven bands indicated above, a supervised classification was run with the random forest algorithm [43], configured with a sample size of 1000 and 100 decision trees. The results of the classifier were evaluated quantitatively, extracting the percentage of coverage per class. The random forest method was used due to its good performance. It also shows the bands that have most influenced the process [44].

Finally, to validate the different classifications, a confusion matrix was performed. The confusion matrix is a quantitative method used to characterize the accuracy of the supervised classification. A table is generated showing the correspondence between the classification result and the defined control regions, so the overall accuracy and kappa index of the classification is calculated. The overall accuracy is determined by dividing the number of correctly classified values by the total number of values. Thus, the overall accuracy indicates the proportion of the correctly mapped reference locations. Overall accuracy is usually expressed as a percentage, with 100% being a perfect classification in which all of the reference locations have been correctly classified. The kappa index measures how the classification results compare to the randomly assigned values. It can take values from 0 to 1. The higher the kappa coefficient, the more accurate the classification. The graph in Figure 7 summarizes the methodology.

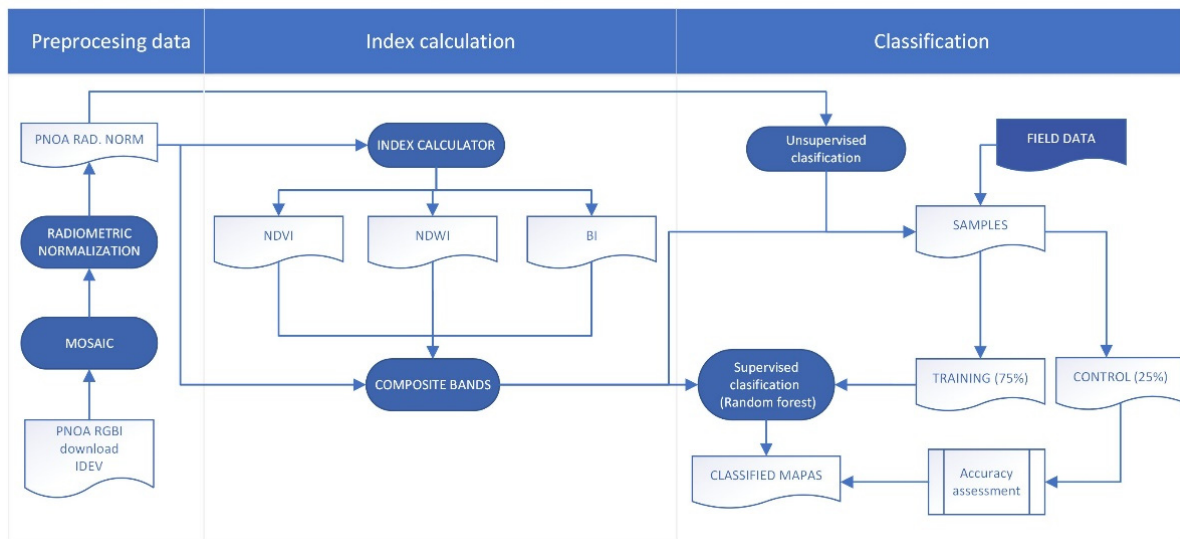


Figure 7. Methodology flowchart for aerial image processing with spectral resolution RGBI (years 2007, 2017, 2019, and 2022).

2.4. Data Set

Different image processing methodologies were applied depending on the type of information analyzed. The information from the aerial images, their purpose, the methodology applied to obtain the information, and the period in which they were used are shown in Table 1.

3. Results and Discussion

3.1. Results

The following information has been structured according to periods. The results are summarized graphically at the end of Section 3.1.

3.1.1. Period 1929–1956: Saltwork Industry

To establish the evolution of vegetation, cover during and immediately after the activity of the saltwork, the aerial photos in Figure 3a,b were used. The images were processed with ArcGis Pro 3.1 and the evaporation pond areas were manually selected. According to this analysis, the percentage of the study area occupied by salt ponds expanded from 36% in 1929 to 82% in 1956. We have assumed that the area outside the evaporation ponds was covered with natural vegetation. According to this, the vegetation cover decreased 46%.

3.1.2. Period 1977–2005: Natural Evolution before the Artificial Irrigation Program

During this period, the salt marsh evolved naturally as an endoreic lagoon subject to periods of flooding due to the accumulation of surface water or the rise of the piezometric level. The aerial photographs from 1977 and 2005 were selected to study the evolution of the vegetation. The procedure was a non-supervised classification with the ISO cluster algorithm and photointerpretation. The panchromatic image from 1977 considered the texture of the image. For example, the ponds in a uniform gray were considered areas with no vegetation, while those in heterogeneous dark colors indicated vegetation. The green areas in the 2005 photo were directly assigned to vegetation. The analysis showed an increase in vegetation from 19% to 38%, as can be seen in Figure 8.

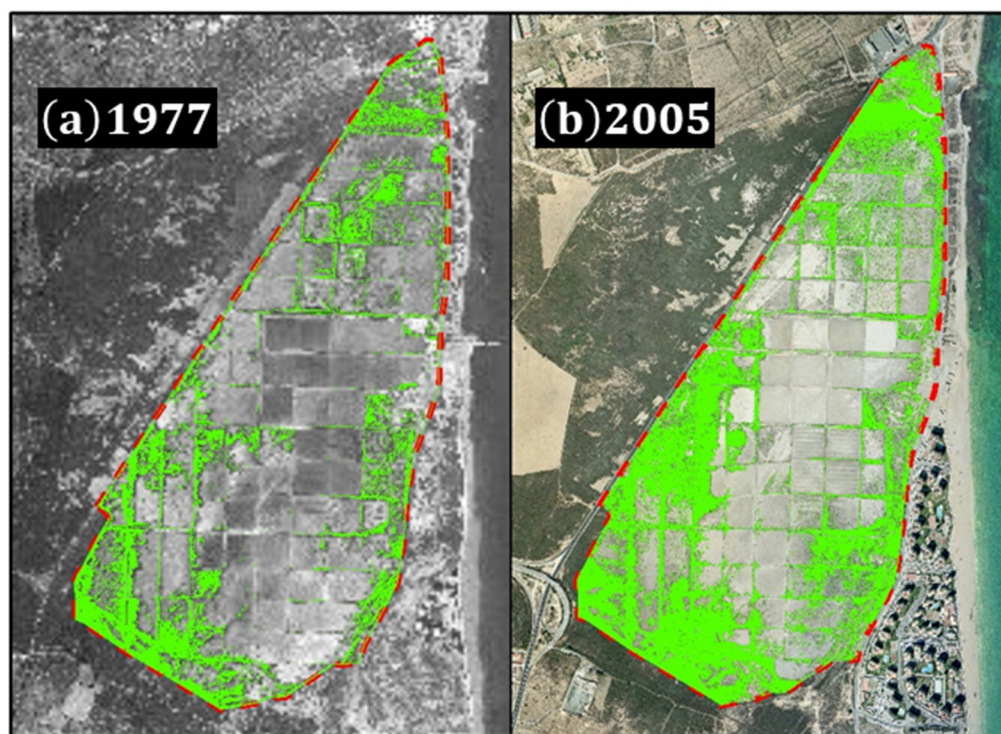


Figure 8. Vegetation using the non-supervised method in aerial photographs from 1977 (a) and 2005 (b). The green areas represent vegetation in the study area.

3.1.3. Period 2007–2022: The Influence of Seawater Recharge on the Salt Marsh

The images from 2007, 2017, 2019, and 2022 were processed using a supervised classification based on the random forest methodology to analyze the evolution of the vegetation in the study area. Two representative pilot ponds have also been considered to highlight the condition of the water and its influence on general vegetation growth. Figure 9 shows the vegetation cover throughout the period. Four areas have been distinguished: dense vegetation, sparse vegetation, bare dark soil, and bare soil. The results are shown in Table 2.

Table 2. Evolution of the percentage of area occupied by the four categories selected for the random forest methodology applied to images from 2007, 2017, 2019, and 2022.

| Time | Bare Soil (%) | Dark Bare Soil (%) | Sparse Vegetation (%) | Dense Vegetation (%) | Total Vegetation (%) | Overall Accuracy (%) | Kappa Index |
|------|---------------|--------------------|-----------------------|----------------------|----------------------|----------------------|-------------|
| 2007 | 25.13 | 29.90 | 35.44 | 9.52 | 45.96 | 80 | 0.73 |
| 2017 | 20.04 | 22.73 | 21.59 | 35.65 | 57.23 | 87.5 | 0.83 |
| 2019 | 12.68 | 28.40 | 25.47 | 33.46 | 58.93 | 82.5 | 0.77 |
| 2022 | 12.10 | 18.46 | 27.23 | 42.16 | 69.38 | 92.5 | 0.9 |

The results of the vegetation evolution (including dense and sparse) during this period were 45.96% in 2007, 57.23% in 2017, 58.93% in 2019, and 69.38% in 2022. The increase in vegetation cover for this period was around 24%. The total increase in vegetation cover due to natural evolution and artificial recharge (period 1970–2022) is around 50% (from 19% to 69.38%).

Factors related to meteorology (rain distribution), biology (seasonal vegetation cycle), and human activity (artificial irrigation) might also influence the results. The information provided in the analysis of the two pilot ponds throughout the period has led us to some conclusions about this (Figure 10).



Figure 9. Results of analysis on vegetation cover using random forest during the period 2007–2022.

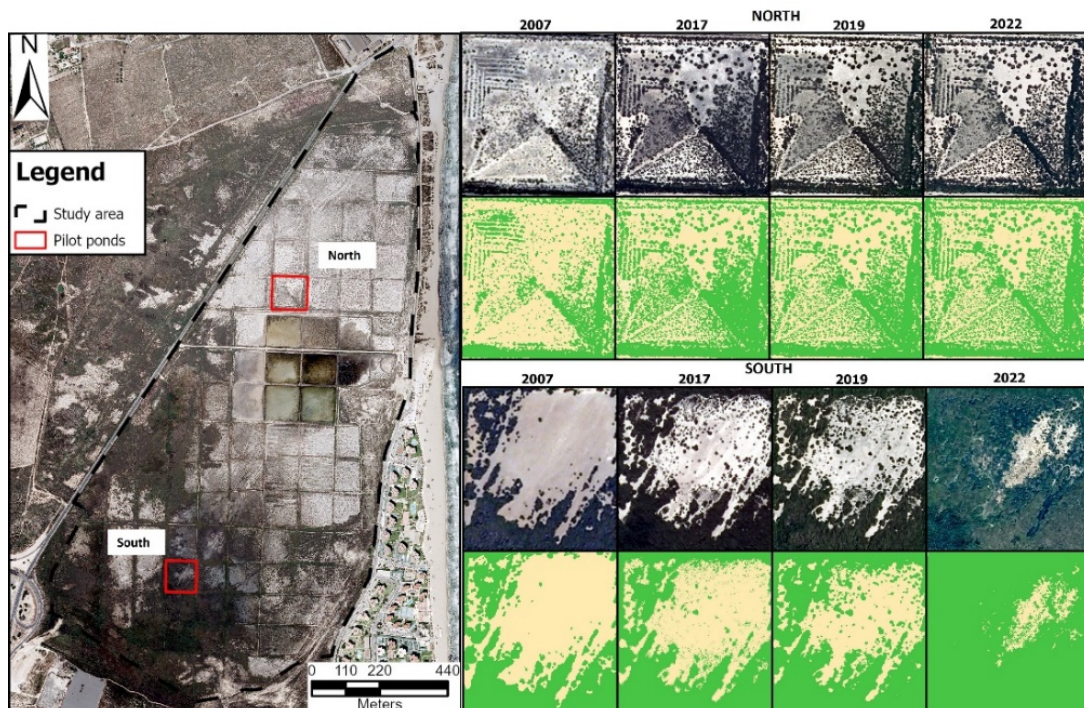


Figure 10. Results of analysis on vegetation cover in two pilot ponds located in a seawater-influenced area (north) and freshwater-influenced area (south) during the period 2007–2022 using random forest. Soil with vegetation (dense and sparse, green marked) and soil without vegetation (yellow marked).

The results (Table 3) were separated into two categories: soil with vegetation (dense and sparse) and soil without vegetation (bare and dark bare soil).

Table 3. Evolution of the distribution of two categories (dense and sparse vegetation and bare and dark bare soil) selected for the random forest methodology applied to two pilot ponds in the images from 2007, 2017, 2019, and 2022.

| Time | Seawater-Influenced Pond (North) | | Freshwater-Influenced Pond (South) | | Differences |
|------|----------------------------------|----------|------------------------------------|----------|----------------|
| | Vegetation (%) | Soil (%) | Vegetation (%) | Soil (%) | Vegetation (%) |
| 2007 | 36.7 | 63.3 | 46.2 | 53.8 | 10 |
| 2017 | 54.5 | 45.5 | 67.8 | 32.2 | 14 |
| 2019 | 50.3 | 49.7 | 66.1 | 33.9 | 16 |
| 2022 | 52 | 48 | 93.7 | 6.3 | 41 |

The pond located near the rainstorm tank (freshwater-influenced) showed an increase throughout the period of around 47% in the area occupied by vegetation, while the pond located in the north of the artificially irrigated area (seawater-influenced) showed an increase throughout the period of around 16% in the area occupied by vegetation.

3.1.4. Period 2009–2016. A Proposal to Monitor the Spread of Tall Vegetation Specimens

The data provided by the nDSM of vegetation made via LiDAR was used to study the spread of reedbeds. Table 4 shows the results of the nDSM of vegetation from 2009, with a spatial resolution of 2.5 m and 0.4 m precision in altimetry, and those from 2016, with a spatial resolution of 1 m and 0.2 m precision in altimetry.

Table 4. Distribution of vegetation height according to data provided by nDSM of vegetation made with LiDAR.

| Height (m) | NDSM V 2009 | NDSM V 2016 |
|------------------------|-------------|-------------|
| without vegetation = 0 | 98.49% | 88.68% |
| with vegetation > 0 | 1.51% | 11.32% |
| $x \leq 1$ | 1.42% | 11.18% |
| $x > 1$ | 0.09% | 0.14% |

The percentage of the area occupied by tall species varied from 0.09% to 0.14% between the years 2009 and 2016 (marked in red in Figure 11), so the value, according to the LiDAR data, is duplicated.

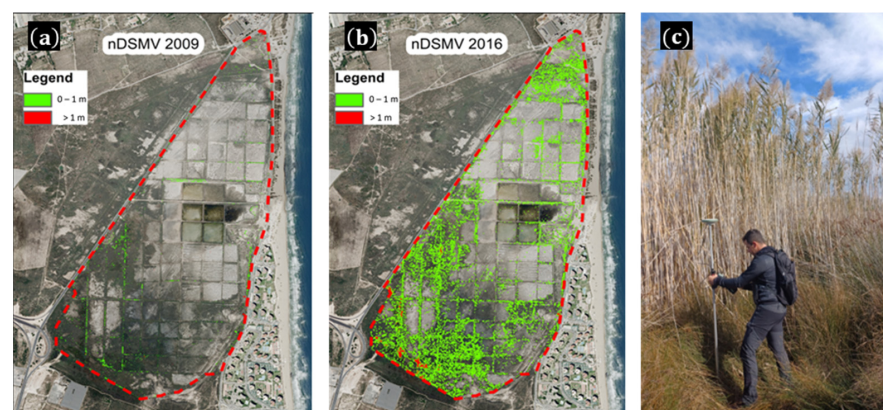


Figure 11. Vegetation height distribution based on data provided by nDSM of vegetation made with LiDAR in 2009 (a) and 2016 (b). *Phragmites australis* and *Juncus* in the south of the study area, next to the drainage system of the rainstorm tank at the Alicante Airport (c).

3.1.5. The Spread of Tall Vegetation Specimens According to 2023 Field Surveys

The field surveys carried out in October 2023 aimed to define the area where *Phragmites australis* prevailed among other species (Figures 6a and 11c). Areas where the specimens were spaced apart from one another were not included (Figure 6b).

The spread of predominant *Phragmites australis* reached 21.2% of the study area (Figure 12). The information related to the reedbed spread in the monitoring field from 2005 (Figure 4b) was also included in the figure (9%), so the increase in the total area can easily be observed (around 12%).

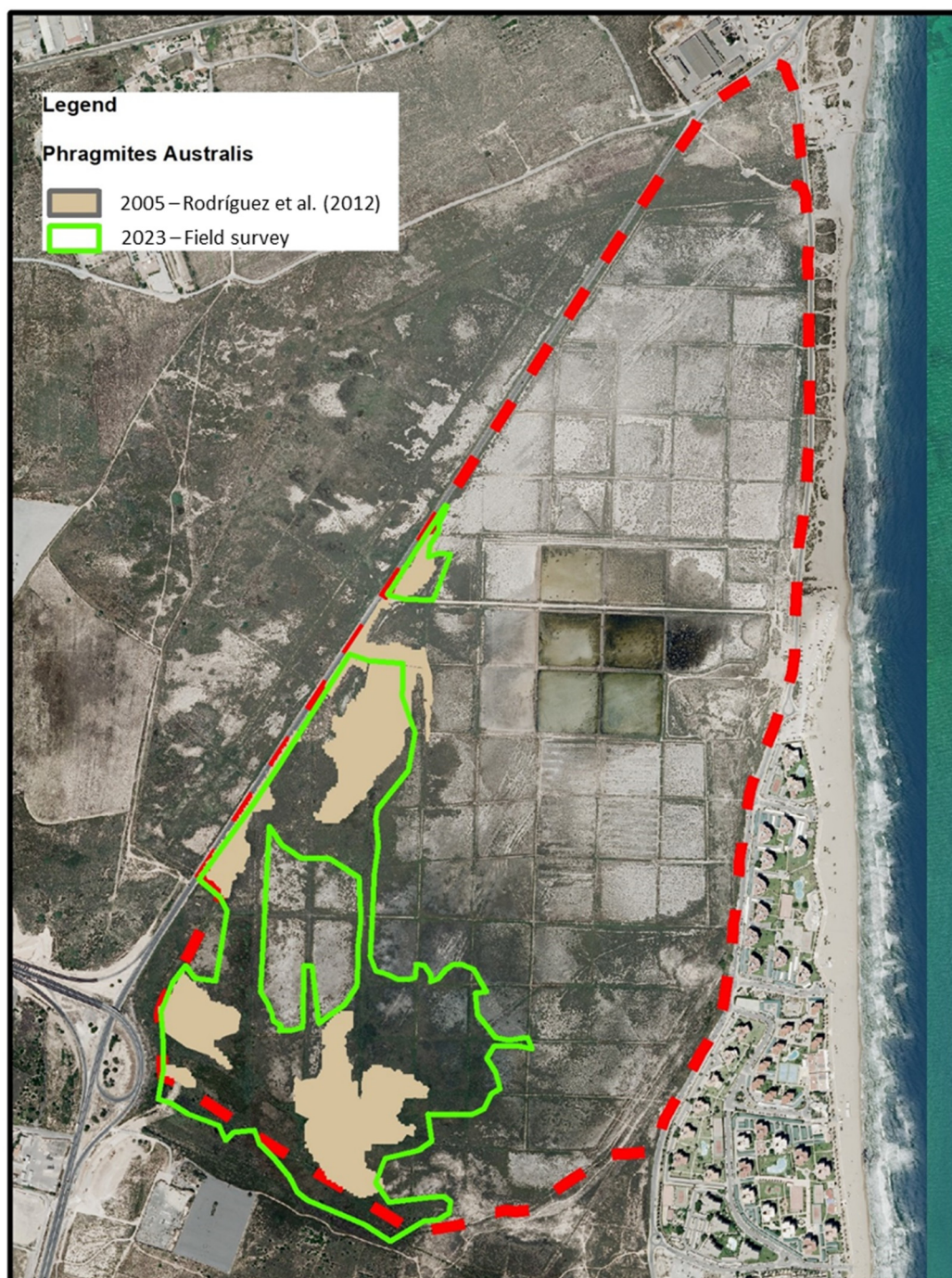


Figure 12. Area with a predominance of *Phragmites australis* (reedbed) from the 2005 (in brown [32]) and 2023 (green line) field surveys.

The results of the whole period analyzed (1929–2023) are summarized in Figure 13.

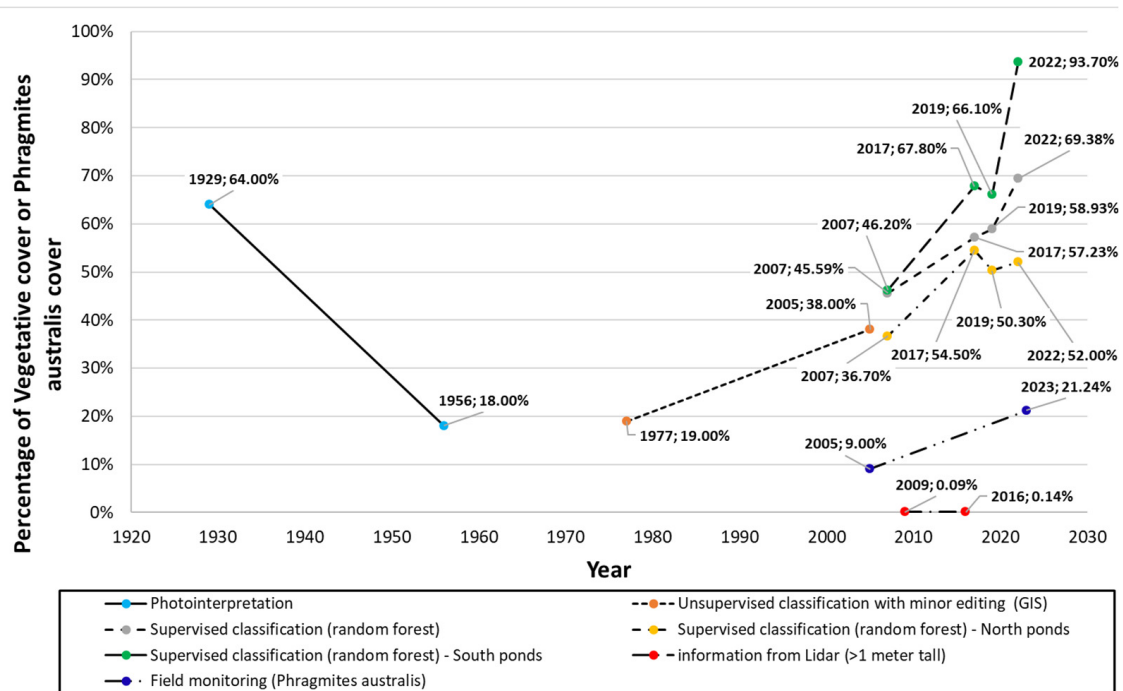


Figure 13. Graph showing the vegetation cover and *Phragmites australis* extension (%) in the study area obtained from aerial image processing and field monitoring during the period 1929–2023 in the Agua Amarga salt marsh.

3.2. Results and Discussion

Before discussing the results, we should establish some determining aspects related to the information of the aerial images. The purpose of the images used as base data in this work (Table 1) was originally to produce orthophotos. The images are orthorectified from orientations obtained with aerotriangulation processes and from the digital terrain model revised and updated to the date the flight was made. The continuous image has been obtained by making a mosaic and final radiometric adjustment of the whole work. This last step was not performed on the downloaded images.

National and regional administrations make these images freely available as a cartographic base. Since 2007, the images have been acquired with 4-band multispectral cameras for visible and near-infrared, so the images were obtained in false color and with high spatial resolution. As the objective was not remote sensing, there are several drawbacks that influence the results of this work: (i) the images are not radiometrically corrected since they were of the same area on different days; (ii) the images were taken annually, but on different dates (up to 3 months apart), so the phenological state of the vegetation is different; (iii) the multispectral cameras are of three different models, with different peak spectral values of the bands; and (iv) the spatial resolution in 2007 (0.5 m) was different from the other years (0.25 m).

Despite these limitations, the information is free data that can be used for remote sensing research, as we deal with in this work.

Regarding the result of the 1929–1956 period, we based the existence of natural vegetation cover previous to building the evaporation ponds on the thesis set by Box Amorós [26]. The comparison with field data results can first be applied from 2005, when the supplementary information related to the vegetation distribution from the field surveys has been provided by the vegetation map in Figure 4b. According to this map, 54% of the area was covered with vegetation (mainly *Suaeda vera*, *Sarcocornia fruticosa*, *Arthrocnemum macrostachyum*, and *Phragmites australis*). Compared to the analysis made by the non-

supervised procedure, there is a difference of around 17%. The data obtained from the field surveys consider the concept “area with predominance of” (Figure 14).

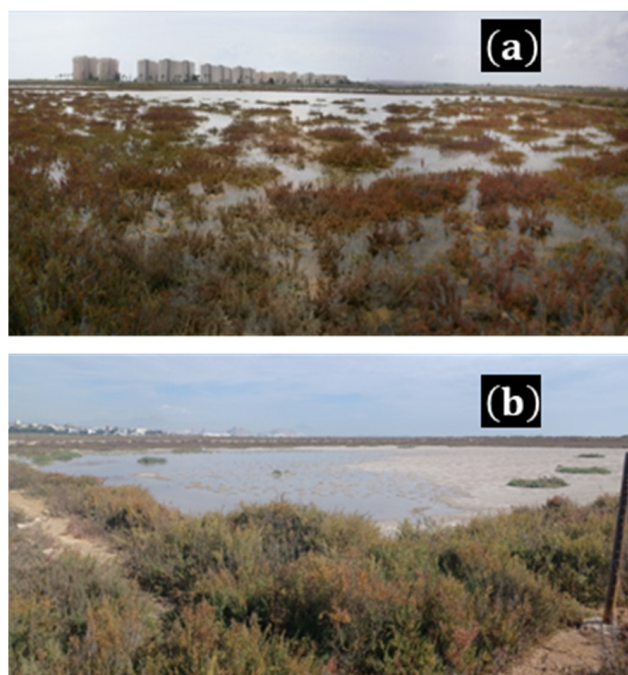


Figure 14. (a) Panoramic view of a flooded pond with *Arthrocnemum macrostachyum* growing in dispersed patches (area covered with vegetation according to field data). (b) Artificial irrigation pond with *Sarcocornia fruticosa* growing in a dense stand on the periphery and dispersed patches of *Arthrocnemum macrostachyum* growing inside with extensive areas of bare soil among the specimens (area not covered with vegetation but with a predominance of *Arthrocnemum macrostachyum* according to the field data).

This does not mean that the vegetation covers the whole area. Therefore, the aerial image is more accurate in distinguishing between areas with and without vegetation.

According to the information obtained from field monitoring and aerial photo geopositioning during the period 2012–2022, the increase in vegetation cover was 10–25% [37]. This result confirmed the positive tendency. The differences, as mentioned in the interpretation of Figure 4b, lie in the concept “area with predominance of” applied in the field surveys, which includes the percentage of soil without vegetation located between nearby specimens. This surface is considered soil without vegetation in the aerial image processing, which explains why the results from the field surveys generally show higher percentages of vegetation cover.

Considering the disadvantages due to the origin and purpose of the images mentioned in Section 2, acceptable results have been achieved in terms of overall accuracy and the kappa index for each of the four images, as shown in Table 2 [39]. The oldest image (from 2007) has the worst results, with 80% and 0.73, respectively. The lower resolution in this year (0.5 m vs. 0.25 m in 2017–2022), explains this difference.

As concluded for the whole study area, the general tendency is positive, and the vegetation cover has increased in the two ponds selected to oversee the influence of seawater vs. fresh water. Moreover, the pond located in the freshwater-influenced area shows more extensive vegetation cover in all of the years studied. This difference increases throughout the period from 10 to 41%.

The pattern in the pond in the freshwater-influenced area fluctuates sharply in the evolution of vegetation cover (an increase of 26% from 2019 to 2022). This is not a permanent situation because, as was verified during the field monitoring, the presence of sporadic

seasonal plant growth might influence the results. In fact, this exceptional emergence of vegetation is related to the special rain event occurring in March–May 2022 (350 mm, Figure 5). Near the seawater-recharge-influenced pond, with the presence of permanent salt marsh vegetation, the pattern is more stable, and the increase in vegetation cover was around 2% for the same period.

The results from the LiDAR data have been influenced by some factors. Improved resolution has allowed us to better identify the vegetation cover, going from a poor result in 2009 (1.51%) to a more accurate one in 2016 (11.32%), mainly due to vegetation of under one meter. The absolute results (vegetation cover $x < 0$) are different from those obtained from random forest. The increase in vegetation cover related to the whole study area is around 10% with LiDAR and around 20% with random forest for the same period (2007–2017). The resolution of the LiDAR image clearly influences the results.

The first data supporting the existence of *Phragmites australis* dates to 2005 (Figure 4b). The area identified as reedbed based on the field surveys was calculated as covering 9%. Again, the resolution of the LiDAR image clearly influences the results obtained in 2009 and 2016, since the field survey in 2023 (21.2% of predominant *Phragmites australis* in the study area) notes an increase of around 12% from 2005. The spread of the reedbeds in natural salt marshes due to the influence of fresh water has also been noted near the Mar Menor Lagoon, located 50 km south of the Agua Amarga salt marsh [25].

Although *Phragmites australis* was the most representative of the taller species in the study area, other tall species, such as *Nicotiana glauca*, *Juncus*, and *Pistacia lentiscus*, might contribute to the calculation made from the LiDAR data. This demonstrates the complementarity between the information from the field surveys and from aerial image processing [9].

To improve the accuracy and the possibilities of the LiDAR data, remote sensing from unmanned aerial vehicles (UAVs) offers alternatives for detecting changes on a small scale with high spatial resolution [45], incorporating both LiDAR and multispectral cameras. The combination of the two types of data can be decisive in differentiating among plant species of different heights in the study area [46].

4. Final Comments and Conclusions

The Agua Amarga salt marsh and the coastal aquifer connected to it have been subject to anthropogenic intervention since 1925. These interventions were aimed at exploiting seawater as a natural resource: a source of salt in the saltwork industry and a source of fresh water after the desalination procedure. These two actions modified the land surface, vegetation cover, groundwater flow, and salinity.

To mitigate some of these impacts, an artificial recharge program has been implemented since 2005. The restoration of the aquifer piezometry and an increase in typical salt marsh vegetation cover have been verified by the field surveys monitoring the salt marsh ecosystem. Thus, implementing these measures converts the process into a sustainable one since a natural resource (groundwater) has been exploited while the protected salt marsh has benefited.

In this work, we have made a complete study of the vegetation cover since the beginning of human intervention in the Agua Amarga salt marsh, using aerial image processing with different methodologies.

The photointerpretation of images from 1929 and 1956 showed a decrease in natural vegetation cover from 64% to 18% (46%), respectively, when the salt works were fully operational. After 1969, the salt industry closed, so before the next artificial seawater recharge took place in 2008, 39 years of natural evolution had occurred. The unsupervised classification of aerial images from 1977 and 2005 shows an increase in vegetation cover from 19% to 38% during this period of natural evolution. Thus, the effect of the artificial seawater recharge on vegetation was studied during the period 2007–2022 using supervised classification based on the random forest methodology applied to 4-band RGBI images from 2007, 2017, 2019, and 2022. This resulted in a total increase in vegetation cover due to natural evolution and artificial recharge of 50% from 1977 to 2022. Applying the same

methodology during the same period to two pilot ponds selected to monitor the influence of fresh water (a pond located in the south, next to the discharge of the stormwater tank at the Alicante Airport) and seawater (a pond located in the north next to the seawater irrigation system) resulted in an increase in vegetation cover from 46.2% to 93.7% in the south and 36.7% to 52.0% in the north, demonstrating a more stable and positive pattern of permanent typical salt marsh vegetation.

Finally, information from LiDAR was used to differentiate vegetation according to height in 2009 and 2016. This procedure might be of interest for studies on the spread of invasive species like *Phragmites australis*. The vegetation covers of species higher than 1 m increased (from 0.09% to 0.14%). Resolution was found to be the most limiting aspect of this procedure, which could be addressed by incorporating unmanned aerial vehicles (UAVs) with high spatial resolution, and LiDAR and multispectral cameras.

The comparison of these results with those obtained from field monitoring highlights the advantages and the complementarity of combining both procedures when analyzing the evolution of specific species or the permanent vegetation cover in the salt marsh. The information gathered from field monitoring provided higher values of vegetation cover (54% vs. 38% in 2005). This is because the bare soil between predominant specimens is neglected in field surveys but not in image processing, so the results from aerial images are more accurate. Extending field monitoring is limited by accessibility, while the aerial image covers the whole study area. The spread of *Phragmites australis* was verified by comparing the results of field monitoring carried out in 2005 and 2023 (from 9.0% to 21.2%, respectively). Other taller species, such as *Nicotiana glauca*, *Juncus*, and *Pistacia lentiscus*, were not considered in field monitoring, but they would have been included in a procedure based on LiDAR data. Similarly, the sporadic emergence of seasonal plants was not eliminated from the information obtained with random forest in the 2022 image (pilot pond located in the south with 97.3% vegetation cover). Field monitoring is again required to differentiate these species.

Free aerial images provided by public administrations might be a source of information for researchers despite their limitations. Applying these images to vegetation cover in the Agua Amarga salt marsh proved to be an additional tool to control the vegetation cover during the period 1929–2022 and a potential source of information that could help control the spread of invasive species in a scenario where water management measures are implemented.

Author Contributions: Conceptualization, I.A.; Methodology, J.M.S., I.A. and M.A.; Software, J.M.S. and M.A.; Validation, I.A., J.Á.-R. and J.A.J.-V.; Formal analysis, J.M.S., I.A., M.A., J.Á.-R. and J.A.J.-V.; Investigation, J.M.S., I.A., M.A. and J.A.J.-V.; Resources, J.M.S. and J.Á.-R.; Data curation, I.A., M.A. and J.A.J.-V.; Writing—original draft, I.A.; Writing—review & editing, I.A. and J.A.J.-V.; Visualization, I.A.; Supervision, I.A. and M.A. All authors have read and agreed to the published version of the manuscript.

Funding: Financial support for monitoring field surveys and access to the information in this research were provided by MCT.

Data Availability Statement: Data is contained within the article.

Conflicts of Interest: The authors declare no conflict of interest.

References

1. Hürlimann, M.; Guo, Z.; Puig-Polo, C.; Medina, V. Impacts of future climate and land cover changes on landslide susceptibility: Regional scale modelling in the Val d’Aran region (Pyrenees, Spain). *Landslides* **2022**, *1–20*, 99–118. [[CrossRef](#)]
2. Machado Toffolo, M.; Grilli, F.; Prandi, C.; Goffredo, S.; Marini, M. Extreme Flooding Events in Coastal Lagoons: Seawater Parameters and Rainfall over A Six-Year Period in the Mar Menor (SE Spain). *J. Mar. Sci. Eng.* **2022**, *10*, 1521. [[CrossRef](#)]
3. TuTiempo.net. Clima Alicante/El Altet. Available online: <https://www.tutiempo.net/clima/ws-83600.html> (accessed on 5 October 2023).
4. Espinar, J.L. 1420. Matorrales Halófilos Mediterráneos y Termoatlánticos (Sarcocornetea Fruticosi). In *Bases Ecológicas Preliminares Para la Conservación de los Tipos de Hábitat de Interés Comunitario en España*, 1st ed.; Ministerio de Medio Ambiente y Medio Rural y Marino; Secretaría General Técnica; Centro de Publicaciones: Madrid, Spain, 2009.

5. Gagnon Lupien, N.; Gauthier, G.; Lavoie, C. Effect of the invasive common reed on the abundance, richness and diversity of birds in freshwater marshes. *Anim. Conserv.* **2015**, *18*, 32–43. [CrossRef]
6. Tougas-Tellier, M.A.; Morin, J.; Hatin, D.; Lavoie, C. Freshwater wetlands: Fertile grounds for the invasive *Phragmites australis* in a climate change context. *Ecol. Evol.* **2015**, *5*, 3421–3435. [CrossRef] [PubMed]
7. Higginson, W.; Cobb, A.; Tschierschke, A.; Dyer, F. The role of environmental water and reedbed condition on the response of *Phragmites australis* reedbeds to flooding. *Remote Sens.* **2022**, *14*, 1868. [CrossRef]
8. Onojeghuo, A.O.; Blackburn, G.A. Mapping reedbed habitats using texture-based classification of QuickBird imagery. *Int. J. Remote Sens.* **2011**, *32*, 8121–8138. [CrossRef]
9. Onojeghuo, A.O.; Blackburn, G.A. Optimising the use of hyperspectral and LiDAR data for mapping reedbed habitats. *Remote Sens. Environ.* **2011**, *115*, 2025–2034. [CrossRef]
10. Blount, T.R.; Carrasco, A.R.; Cristina, S.; Silvestri, S. Exploring open-source multispectral satellite remote sensing as a tool to map long-term evolution of salt marsh shorelines. *Estuar. Coast. Shelf Sci.* **2022**, *266*, 107664. [CrossRef]
11. Jensen, J.R. *Remote Sensing of the Environment: An Earth Resource Perspective*; Prentice Hall: Upper Saddle River, NJ, USA, 2006.
12. Sun, T.; Cheng, W.; Abdelkareem, M.; Al-Arifi, N. Mapping Prospective Areas of Water Resources and Monitoring Land Use/Land Cover Changes in an Arid Region Using Remote Sensing and GIS Techniques. *Water* **2022**, *14*, 2435. [CrossRef]
13. Li, Y.; Abdelkareem, M.; Al-Arifi, N. Mapping Potential Water Resource Areas Using GIS-Based Frequency Ratio and Evidential Belief Function. *Water* **2023**, *15*, 480. [CrossRef]
14. Lobell, D.B.; Ortiz-Monasterio, J.I.; Asner, G.P.; Naylor, R.L.; Falcon, W.P. Combining field surveys, remote sensing, and regression trees to understand yield variations in an irrigated wheat landscape. *Agron. J.* **2005**, *97*, 241–249. [CrossRef]
15. Lemenkova, P.; Debeir, O. Computing Vegetation Indices from the Satellite Images Using GRASS GIS Scripts for Monitoring Mangrove Forests in the Coastal Landscapes of Niger Delta, Nigeria. *J. Mar. Sci. Eng.* **2023**, *11*, 871. [CrossRef]
16. Jamali, A.A.; Naeni, M.A.M.; Zarei, G. Assessing the expansion of saline lands through vegetation and wetland loss using remote sensing and GIS. *Remote Sens. Appl. Soc. Environ.* **2020**, *20*, 100428. [CrossRef]
17. Tiwari, S.K.; Prasada Rao, G.; Sundar, B. Assessment of Vegetation Dynamics of Paddy Crop Using “TIMESAT” and Remote Sensing and GIS Techniques in Command Areas. In *Advances in Water Resource Planning and Sustainability*; Springer Nature Singapore: Singapore, 2023; pp. 23–37.
18. Salari, A.; Zakaria, M.; Nielsen, C.C.; Boyce, M.S. Quantifying tropical wetlands using field surveys, spatial statistics and remote sensing. *Wetlands* **2014**, *34*, 565–574. [CrossRef]
19. Belluco, E.; Camuffo, M.; Ferrari, S.; Modenese, L.; Silvestri, S.; Marani, A.; Marani, M. Mapping salt-marsh vegetation by multispectral and hyperspectral remote sensing. *Remote Sens. Environ.* **2006**, *105*, 54–67. [CrossRef]
20. Zhang, M.; Ustin, S.L.; Rejmankova, E.; Sanderson, E.W. Monitoring Pacific coast salt marshes using remote sensing. *Ecol. Appl.* **1997**, *7*, 1039–1053. [CrossRef]
21. Peña-Barragán, J.M.; Ngugi, M.K.; Plant, R.E.; Six, J. Object-based crop identification using multiple vegetation indices, textural features and crop phenology. *Remote Sens. Environ.* **2011**, *115*, 1301–1316. [CrossRef]
22. Rouse, J.W.; Haas, R.H.; Schell, J.A.; Deering, D.W. Monitoring vegetation systems in the Great Plains with ERTS. *NASA Spec. Publ.* **1974**, *351*, 309.
23. Gao, B.C. NDWI—A normalized difference water index for remote sensing of vegetation liquid water from space. *Remote Sens. Environ.* **1996**, *58*, 257–266. [CrossRef]
24. Hladik, C.; Alber, M. Classification of salt marsh vegetation using edaphic and remote sensing-derived variables. *Estuar. Coast. Shelf Sci.* **2014**, *141*, 47–57. [CrossRef]
25. Carreño, M.F.; Esteve, M.A.; Martínez, J.; Palazón, J.A.; Pardo, M.T. Habitat changes in coastal wetlands associated to hydrological changes in the watershed. *Estuar. Coast. Shelf Sci.* **2008**, *77*, 475–483. [CrossRef]
26. Box Amorós, M. Las Zonas Húmedas de la Provincia de Alicante y los Procesos de Intervención Antrópica. Ph.D. Thesis, Universitat d’Alacant-Universidad de Alicante, Alicante, Spain, 3 December 1985.
27. Confederación Hidrográfica del Segura. Directorio de Servicios Web de Mapas WMS y WMTS. Vuelo de 1929–1930 Ruiz de Alda. Available online: <https://www.chsegura.es/va/cuenca/cartografia/servicios-web-de-mapas/directorio-de-servicios-web-de-mapas/> (accessed on 13 December 2023).
28. Geoportal de la Infraestructura de Datos Espaciales de España. Ortofotos del Vuelo Americano (serie B) 1956–1957. Available online: <https://www.idee.es/csw-inspire-idee/srv/spa/catalog.search?#/metadata/spaignAMSserieB> (accessed on 4 December 2023).
29. Confederación Hidrográfica del Segura. Directorio de Servicios Web de Mapas WMS y WMTS. Vuelo de 1973–1986 Interministerial. Available online: <https://www.chsegura.es/va/cuenca/cartografia/servicios-web-de-mapas/directorio-de-servicios-web-de-mapas/> (accessed on 11 December 2023).
30. Gobierno Valenciano. Acuerdo [2002/A9833]. Aprobación del Catálogo de Zonas Húmedas de la Comunidad Valenciana; DOGV num. 4336. 10 September 2002. Available online: [https://dogv.gva.es/es/eli/es-vc/a/2002/09/10/\(1\)/](https://dogv.gva.es/es/eli/es-vc/a/2002/09/10/(1)/) (accessed on 16 December 2023).
31. Infraestructura de Datos Espaciales de España. WMTS de Ortoimágenes de España (Satélite Sentinel2 y ortofotos del PNOA MA). Available online: https://www.idee.es/csw-codsi-idee/srv/api/records/spaignwmts_pnoa-ma (accessed on 16 December 2023).

32. Rodríguez Estrella, T.; Álvarez-Rogel, J.; Sánchez Lizaso, J.L.; Alhama Manteca, I.; González-Alcaraz, M.N.; Fernández Torquemada, Y.; Montero Meléndez, J. Gestión Ambiental De Las Desaladoras De La Mancomunidad De Los Canales Del Taibilla En Alicante. In Proceedings of the IX Congreso Internacional Aedyr, Madrid, Spain, 12–15 November 2012.
33. Rodríguez-Estrella, T.; Pulido-Bosch, A. Methodologies for abstraction from coastal aquifers for supplying desalination plants in the south-east of Spain. *Desalination* **2009**, *249*, 1088–1098. [[CrossRef](#)]
34. Navarro, R.; Sanchez Lizaso, J.L. Mitigation cost of desalination intake impact on coastal wetlands. *Desalin. Water Treat* **2021**, *224*, 136–143. [[CrossRef](#)]
35. Manteca, I.A.; Estrella, T.R.; Alhama, F. Hydric restoration of the Agua Amarga Salt Marsh (SE Spain) affected by abstraction from the underlying coastal aquifer. *Water Resour. Manag.* **2012**, *26*, 1763–1777. [[CrossRef](#)]
36. González-Alcaraz, M.N.; Aránega, B.; Tercero, M.C.; Conesa, H.M.; Álvarez-Rogel, J. Irrigation with seawater as a strategy for the environmental management of abandoned solar saltworks: A case-study in SE Spain based on soil–vegetation relationships. *Ecol. Eng.* **2014**, *71*, 677–689. [[CrossRef](#)]
37. Alhama, I.; García-Ros, G.; González-Alcaraz, M.N.; Álvarez-Rogel, J. Long-term artificial seawater irrigation as a sustainable environmental management strategy for abandoned solar salt works: The case study of Agua Amarga salt marsh (SE Spain). *Catena* **2022**, *217*, 106429. [[CrossRef](#)]
38. Muñoz-Reinoso, J.C.; Jordán, R.V.; Tejada-Tejada, M. Analysis of Spatio-Temporal Changes in the Vegetation Cover of the Coastal Landscape of Doñana. *J. Coast. Res.* **2020**, *95*, 113–117. [[CrossRef](#)]
39. Richards, J.A.; Jia, X. Clustering and Unsupervised Classification. In *Remote Sensing Digital Image Analysis: An Introduction*; Springer: New York, NY, USA, 1990.
40. Ball, D.; Soto-Berelov, M.; Young, P. Historical seagrass mapping in Port Phillip Bay, Australia. *J. Coast. Conserv.* **2014**, *18*, 257–272. [[CrossRef](#)]
41. Canty, M.J.; Nielsen, A.A. Automatic radiometric normalization of multitemporal satellite imagery with the iteratively re-weighted MAD transformation. *Remote Sens. Environ.* **2008**, *112*, 1025–1036. [[CrossRef](#)]
42. Mathieu, R.; Pouget, M.; Cervelle, B.; Escadafal, R. Relationships between satellite-based radiometric indices simulated using laboratory reflectance data and typical soil color of an arid environment. *Remote Sens. Environ.* **1998**, *66*, 17–28. [[CrossRef](#)]
43. Breiman, L. Random forests. *Mach. Learn.* **2001**, *45*, 5–32. [[CrossRef](#)]
44. Liaw, A.; Wiener, M. Classification and regression by random Forest. *R News* **2002**, *2*, 18–22.
45. Tiškus, E.; Vaičiūtė, D.; Bučas, M.; Gintauskas, J. Evaluation of common reed (*Phragmites australis*) bed changes in the context of management using earth observation and automatic threshold. *Eur. J. Remote Sens.* **2023**, *56*, 2161070. [[CrossRef](#)]
46. Sankey, J.B.; Sankey, T.T.; Li, J.; Ravi, S.; Wang, G.; Caster, J.; Kasprak, A. Quantifying plant-soil-nutrient dynamics in rangelands: Fusion of UAV hyperspectral-LiDAR, UAV multispectral-photogrammetry, and ground-based LiDAR-digital photography in a shrub-encroached desert grassland. *Remote Sens. Environ.* **2021**, *253*, 112223. [[CrossRef](#)]

Disclaimer/Publisher’s Note: The statements, opinions and data contained in all publications are solely those of the individual author(s) and contributor(s) and not of MDPI and/or the editor(s). MDPI and/or the editor(s) disclaim responsibility for any injury to people or property resulting from any ideas, methods, instructions or products referred to in the content.